ANTICANCER RESEARCH *39*: 1875-1882 (2019)
doi:10.21873/anticanres.13295

Serial Texture Analyses on ADC Maps for Evaluation of Antiangiogenic Therapy in Rat Breast Cancer

SANG MIN LEE[1*], KYUNG WON LEE[2], MIN A. KIM[3], YONG SUB SONG[1], JIN MO GOO[1] and CHANG MIN PARK[1]

[1]*Department of Radiology, Seoul National University College of Medicine, and Institute of Radiation Medicine, Seoul National University Medical Research Center, Seoul, Republic of Korea;*
[2]*Department of Radiology, Seoul National University Bundang Hospital, Seongnam, Republic of Korea;*
[3]*Department of Pathology, Seoul National University College of Medicine, Seoul, Republic of Korea*

Abstract. *Background/Aim: We investigated the correlation between texture features on apparent diffusion coefficient (ADC) maps and histological vascular parameters of FN13762 rat breast cancers after antiangiogenic therapy. Materials and Methods: FN13762 cancer cells were implanted into 30 rats, and bevacizumab was intraperitoneally administered to 15 (treated group). For each rat, magnetic resonance imaging (MRI) was obtained at five time points after baseline examination. Serial texture analyses were performed on ADC maps and extracted texture parameters were correlated with histological vascular parameters. Results: Entropy of the ADC values correlated with microvessel density in the treated group (r=0.493, p=0.06). Hypoxia inducible factor-1 alpha showed the highest correlation coefficient with the 5th percentile ADC value (r=0.844, p<0.001). Vascular endothelial growth factor was significantly correlated with homogeneity on ADC map (r=−0.521, p=0.046). In the control group, no texture features showed significant correlations with histological vascular parameters. Conclusion: ADC map texture features may reflect histological vascular changes after antiangiogenic therapy.*

Angiogenesis, the building of new vessels from pre-existing vessels, plays a critical role in tumor growth, invasion, and metastasis (1). Because deprivation of an adequate blood supply restricts tumor growth, antiangiogenic agents have been validated as an effective therapy for several types of tumors (2-4). However, as antiangiogenic agents may delay tumor growth but not necessarily lead to tumor shrinkage, an unidimensional size measurement according to the response evaluation criteria in solid tumors (RECIST) guidelines (5) may not be sufficient to evaluate the therapeutic effect of these agents. Therefore, imaging techniques that can reflect the pathophysiological processes of these agents have been investigated (6-8).

One of these imaging techniques involves the quantitative analysis of apparent diffusion coefficient (ADC) maps derived from diffusion-weighted magnetic resonance imaging (MRI). Quantitative measurements of ADC can provide information on cellularity and cellular membrane permeability, which have been consistently shown to be useful for monitoring treatment response, detecting residual tumors or recurrence, and predicting the prognosis across various tumors (6, 9-12). Thoeny *et al*. demonstrated that ADC measurements allowed monitoring of the perfusion changes induced by vascular targeting agents in a rat tumor model (8). However, ADC analysis has generally been limited to the measurement of the mean pixel value within a region of interest (ROI) placed on the ADC map.

Recently, texture analysis has been used for lesion characterization, prediction of treatment response, and prognosis (13, 14). Texture analysis is an imaging analysis method involving the extraction of quantitative features based on the distribution of voxel values within a ROI. This analytical method is expected to provide more detailed assessment of lesion characteristics than visual analysis. Although cerebral perfusion skewness and kurtosis changes were associated with early treatment response in patients with newly diagnosed glioblastomas (13), there have been few studies investigating changes in texture features on ADC maps after antiangiogenic treatment. Furthermore, correlations

**Present Address:* Department of Radiology and Research Institute of Radiology, Asan Medical Center, University of Ulsan College of Medicine, Seoul, Republic of Korea.

Correspondence to: Chang Min Park, MD., Department of Radiology, Seoul National University College of Medicine, 101 Daehak-no, Jongno-gu, Seoul 110-744, Republic of Korea. Tel: +82 220720367, Fax: +82 27437418, e-mail: cmpark.morphius@gmail.com

Key Words: Rat, tumor, MR, antiangiogenic agent, MR.

between ADC map texture features and microvessel density (MVD) on histology (which is regarded as the reference standard for measuring tumor angiogenesis) (15), and other vascular markers such as hypoxia inducible factor-1 alpha (HIF-1α) and vascular endothelial growth factor (VEGF, which is associated with angiogenesis) (16-18), have not been investigated.

Therefore, the purpose of our study was to investigate changes in the texture features of ADC maps over serial MR examinations after antiangiogenic therapy, and to determine those texture features reflecting histological vascular markers in FN13762 rat breast cancers.

Materials and Methods

This study was approved by the Animal Care and Use Committee of our Hospital (#13-0322-C0A0).

Animal model. The FN13762 murine mammary carcinoma cell line (American Type Culture Collection, Manassas, VA, USA) was selected as the experimental animal tumor model for this study. FN13762 carcinoma is a spontaneously metastatic syngeneic rat tumor that can be established in female Fischer 344 rats. Both its *in vitro* and *in vivo* growth characteristics have been well defined (19).

Thirty female Fischer 344 rats (Charles River, Sulzbach, Germany) weighing between 250 and 300 g were used in this study. For tumor cell implantation, anesthesia was performed with a solution of zolazepam (5 mg/kg, Zoletil®; Virbac, Carros, France) and xylazine (10 mg/kg, Rompun®; Bayer-Schering Pharma, Berlin, Germany) injected into the hindlimbs. Under the anesthesia, 4×10^5 FN13762 cells suspended in 0.1 ml of Dulbecco's modified Eagle's medium (Cambrex Biosciences, Verviers, France) were inoculated into the muscular layer of the right upper thigh of the rats using a 24-gauge needle. Cellular viability was tested using trypan blue prior to tumor implantation, and yielded a result greater than 90%. All procedures were performed using aseptic technique. At nine days after tumor implantation, tumors were expected to be around 1 cm in the longest dimension, which is a sufficient size for imaging (20) (Figure 1).

Experimental protocol. Nine days after tumor implantation, the 30 Fischer rats were randomly divided into treatment (n=15) and control groups (n=15). Immediately after baseline MR imaging, bevacizumab (Avastin, Genentech, South San Francisco, CA, USA; 20 mg per kg of body weight) was intraperitoneally administered to the treatment group. For each rat in the treatment group, follow-up MR examinations were performed at 2 h, 1 day, 2 days, 5 days, and 9 days after bevacizumab administration, with the same schedule also being applied to the control group. At each follow-up time point, three rats in each group were sacrificed for histopathological assessment.

MR imaging acquisition. MR exams were performed with a 3-T MRI system (TrioTim; Siemens Medical Solutions, Erlangen, Germany) with a 6-channel rat body coil (Stark Contrast, Erlangen, Germany). All MR exams were performed with the rats in a supine position under zolazepam and xylazine anesthesia. After routine localization images were obtained, axial T2-weighted turbo spin echo images (TR/TE, 8930/101 msec; bandwidth, 196 Hz/pixel; flip angle, 120˚; field of view, 100×81 mm; matrix, 192×115; slice thickness, 0.8 mm; number of signals acquired, eight) of the lower half of the rat body were acquired. Then, diffusion-weighted MRI was performed using a free-breathing single-shot echo-planar imaging pulse sequence with diffusion gradients applied in three orthogonal directions. This sequence included the following parameters: TR/TE, 4400/73 ms; bandwidth, 798 Hz/pixel; field of view, 100×100 mm; matrix, 128×128; section thickness, 3 mm; number of signals acquired, eight; and multiple b-values, 0, 25, 50, 75, 100, 200, 400, 800 and 1,000 s/mm^2. The diffusion-weighted MRI covered the entire tumor, and a parallel imaging technique (generalized autocalibrating partially parallel acquisitions; GRAPPA) with a 2-fold acceleration factor was applied to shorten the acquisition time.

Image analysis. Tumor segmentation was performed using in-house software. For each tumor, one radiologist manually drew a ROI covering the entire range of the tumor on the ADC maps. Care was taken to avoid non-tumor tissues on the ADC maps by making reference to the T2-weighted and diffusion-weighted images. After ROI drawing, histogram and texture features were extracted as previously described (20).

Histopathological assessment. After each follow-up MRI session, three rats in each group were sacrificed by means of an intravenous injection of a lethal amount of sodium thiopental (Pentothal; Choong Wae Pharmacy, Seoul, Korea) while they were under deep anesthesia. The rats were then frozen at −70˚C in a plastic frame to maintain their position. One day later, the rats were sectioned in the same plane as the ADC maps.

Pathological specimens were sliced in the transverse plane at 3 mm intervals. After each slice of the specimens had been fixed with 10% phosphate-buffered formaldehyde and embedded in paraffin, pathological specimens (approximately 5 μm thick) were obtained for histological assessment (Figure 2).

For MVD measurement, these pathologic slides were immunohistochemically stained specifically for the endothelial antigen CD34, which is traditionally used to evaluate tumor angiogenesis. One pathologist who was blinded to the results of the MRI counted the number of vessels plus immunoreactive endothelial cells per 200× field in three vascular hot spots within the tumor, and reported the mean number as the final MVD (21). Hot spots were selected at low magnification (40×) according to areas showing the strongest CD34 staining.

These sections were also stained with mouse anti–HIF-1α IgG2b monoclonal antibody (NB100-123, Novus Biologicals, Littleton, CO, USA; dilution, 1:40,000) for evaluation of HIF-1α expression. At least five fields were randomly selected, and the nuclear staining of HIF-1α within tumors was counted under high magnification (400×). HIF-1α expression was defined as positive if nuclear staining was observed in ≥5% of the tumor cells. Simultaneous cytoplasmic staining was excepted, as nuclear HIF-1α determines the functional activity of the HIF-1α complex (22).

VEGF receptor-2 antibody (ab39256, Abcam, Cambridge, MA, USA; dilution, 1:1,000) was used to grade the expression of VEGF in terms of its extent and intensity (23). VEGF-positive brown staining was located in the cytoplasm. The average score over ten fields of vision (400×) was calculated. All microscopic images were captured and saved to a computer using a DP-70 camera with a

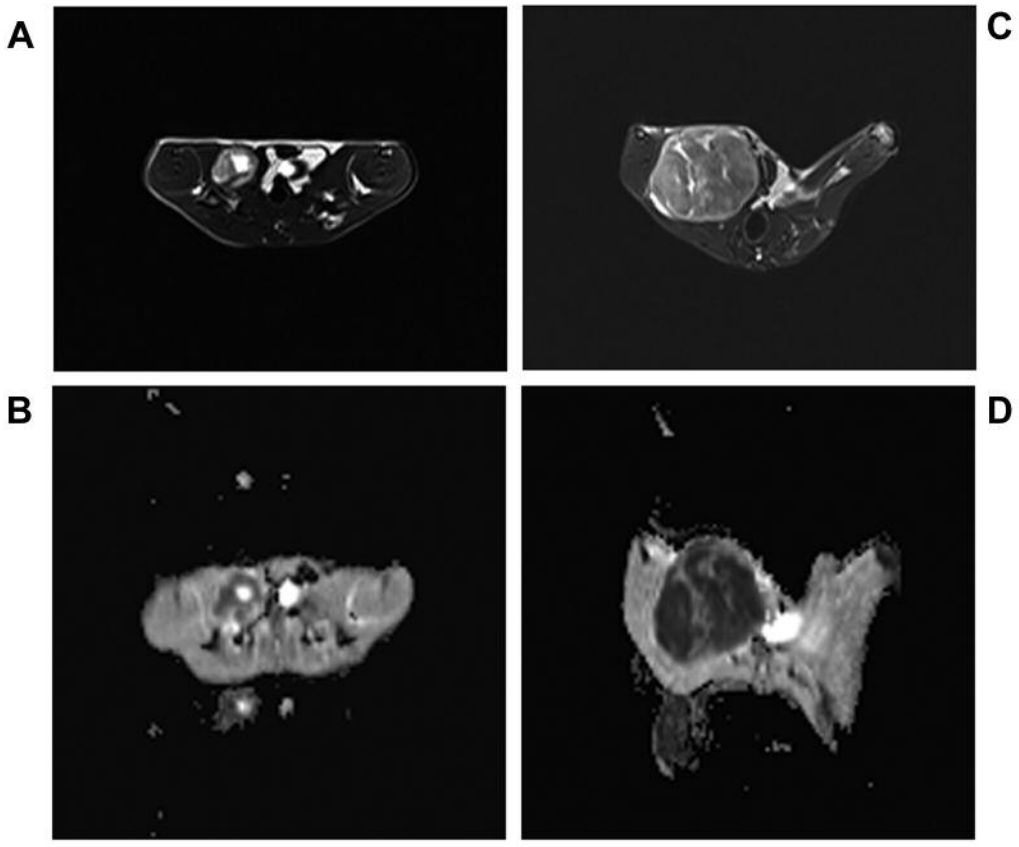

Figure 1. *Tumors in a rat model at baseline and at 9th day follow-up. The tumor was located in the muscular layer of the right upper thigh of the rat. A cystic portion is visible within the tumor. The tumor in the treated rat was 1.5 cm at baseline on the T2-weighted image (A) and corresponding apparent diffusion coefficient map (B). The tumor had grown to 2.4 cm by the 9th day of follow-up (C, D).*

color charge-coupled device sensor mounted on the microscope (Olympus, Tokyo, Japan).

Statistical analysis. The texture features extracted from serial MR acquisitions were compared between the treatment and control groups at each time point. Within the framework of a mixed-effects model, a covariance pattern model, which models a pattern of correlations between repeated measures, was used to compare the mean change of the measured parameters from baseline. In addition, the ADC map texture features were compared with those obtained from the previous examination in each group. The associations between tumor volume and texture features in each group were evaluated using Spearman' s correlation coefficients under the mixed-effects model.

Differences in histological vascular markers between the two groups were compared using the Mann–Whitney test. Associations between texture features and histological vascular markers at each follow-up time point were assessed using Spearman's correlation coefficients. Associations among the histological vascular markers were also evaluated using Spearman's correlation coefficients.

Statistical analyses were performed using SAS statistical software (SAS version 9.4; SAS Institute, Cary, NC, USA). Data are presented as mean±standard deviation. $p<0.05$ was considered to indicate statistical significance.

Results

Changes in texture features during serial follow-ups in the treated and control groups. In both groups, the tumor volumes significantly increased during follow-up (all, $p<0.001$). The differences in tumor volumes between the two groups did not reach statistical significance ($p=0.083$; Table I).

In both groups, the mean tumor ADC values significantly decreased in comparison with baseline ($p=0.014$ in the treated group, and $p<0.001$ in the control group), while the skewness, entropy, and 5th, 10th, 25th, and 50th percentile ADC values of the tumors significantly increased during follow-up ($p=0.001$ for skewness and 50th percentile in the treated group, and $p<0.001$ for the remaining parameters). In the control group, the 75th, 90th, and 95th percentile values also significantly increased during follow-up ($p<0.001$, 0.002, and 0.003, respectively).

However, none of the texture features were significantly different between the two groups (mean values of the tumors on ADC maps, $p=0.431$; skewness, $p=0.753$; kurtosis,

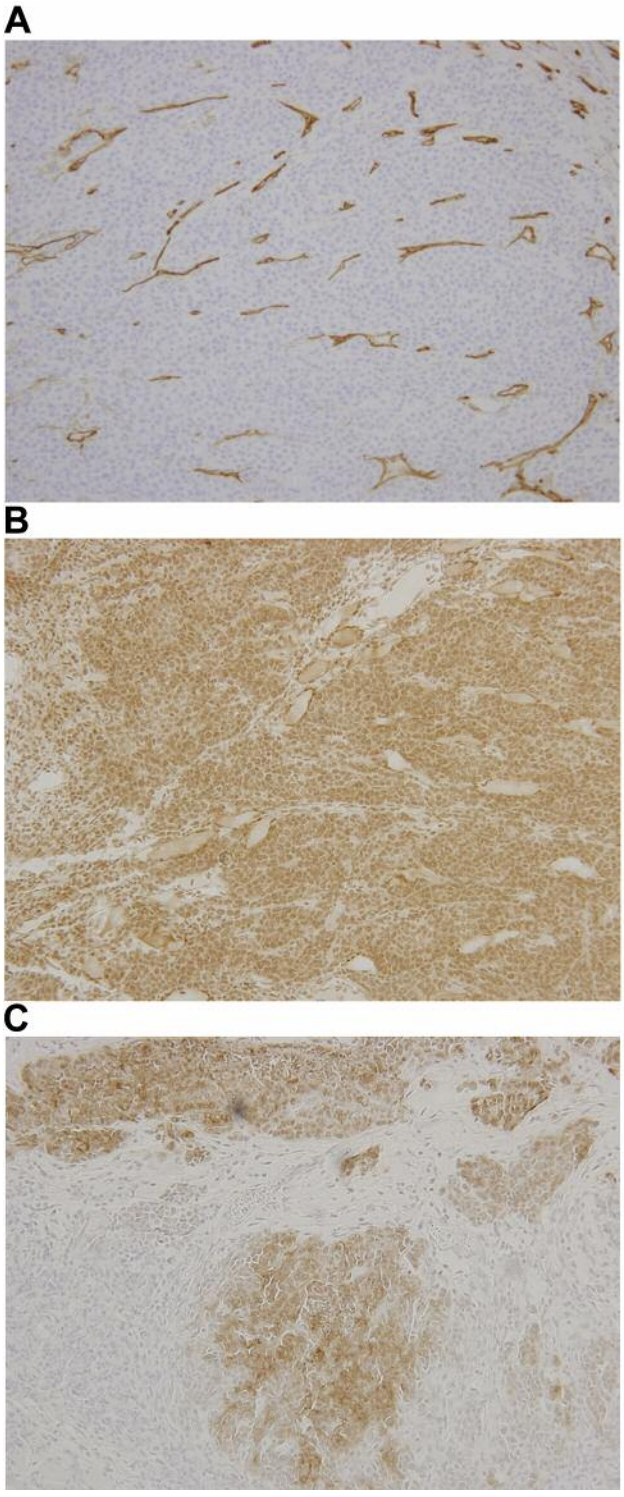

Figure 2. *Quantification of histologically-assessed vascular parameters within a tumor. (A) Microvessel density immunostaining with CD34 antibody highlights vessels (original magnification, 200×). (B) Immunostaining for hypoxia inducible factor-1 alpha, which is mainly identified in the nucleus of cancer cells (original magnification, 400×), and (C) immunostaining for vascular endothelial growth factor (VEGF; original magnification, 400×), which shows as positive brown staining in the cytoplasm.*

p=0.681; entropy, p=0.125; homogeneity, p=0.839; 5th, 10th, 25th, 50th, 75th, 90th, and 95th percentile values, p=0.707, 0.627, 0.968, 0.617, 0.186, 0.271, and 0.252, respectively).

Correlations between texture features and histological vascular parameters. The mean MVD of the treatment group was not significantly different from that in the control group (15.3±4.6 *versus* 15.9±3.9; p=0.604). HIF-1α also showed no significant differences between the two groups (52.0±33.3 *versus* 48.7±10.7; p=0.867). By contrast, VEGF showed significantly higher values in the treatment group than in the control group (33.3±29.9 *versus* 10.7±8.4; p=0.033). Furthermore, in the treatment group, VEGF tended to change a little later in the follow-up period, alongside changes in HIF-1α (Figure 3). No significant correlations were found between the histological vascular parameters in either group (p>0.05).

In the treatment group, MVD showed marginally significant correlations with tumor volume and entropy (r=0.461, p=0.08; r=0.493, p=0.06, respectively). HIF-1α showed significant correlations with 5th, 10th, 25th, 50th, 75th, 90th, and 95th percentile values, mean ADC value, and kurtosis (p<0.05), with the correlation coefficient being highest between the 5th percentile value and HIF-1α (r=0.844). Tumor volume was not significantly correlated with HIF-1α (r=−0.406, p=0.133).

VEGF was significantly correlated with homogeneity (r=−0.521, p=0.046) and showed a marginal association with skewness (r=−0.471, p=0.08). However, tumor volume showed no significant correlation with VEGF (r=−0.04, p=0.883). Table II summarizes the correlations between histological vascular parameters and texture features in the treatment group. In the control group, no texture features showed significant correlations with histological vascular parameters (p>0.05).

Correlations between tumor volume and texture features. When the correlations between tumor volume and texture features were assessed, the mean ADC value, skewness, kurtosis, entropy, and 5th, 10th, 25th, 50th, 75th, and 90th percentile values showed significant correlations in the treatment group (p<0.05), with the correlation coefficient being highest (0.925) between tumor volume and entropy. In the control group, the mean ADC value, skewness, kurtosis, entropy, and 5th, 10th, 25th, and 50th percentile values showed significant correlations with tumor volume (p<0.05), with the correlation coefficient between tumor volume and entropy again being the highest (0.978).

When changes in tumor volume were correlated with changes in texture features, entropy was the only texture parameter showing statistical significance (p<0.001) in the treatment group. In the control group, entropy and

Table I. *Tumor volume and mean ADC values of tumors over serial MR examinations in the treated and control groups.*

	Time points	Treated group		Control group		*p*-Value (between two groups)
Volume (mm^3)	Baseline	760.0±612.4	<0.001	470.1±289.9	<0.001	0.083
	2 hours	786.9±632.1		494.4±290.5		
	1 day	778.2±366.6		828.4±418.6		
	2 days	941.2±426.2		1170.7±630.8		
	5 days	2988.3±1081.5		2154.2±851.9		
	9 days	8028.6±3529.5		13717.7±5477.7		
Mean value on ADC map	Baseline	826.7±264.4	0.014	886.7±107.0	<0.001	0.431
	2 hours	801.9±261.4		862.2±142.1		
	1 day	799.0±129.5		763.6±132.7		
	2 days	734.9±90.9		666.8±93.1		
	5 days	648.4±72.7		576.5±1110.8		
	9 days	687.6±149.9		738.5±116.6		

Data are means±standard deviation.

homogeneity showed significant correlations ($p<0.001$ and $p=0.01$, respectively). In all cases, only entropy remained significantly correlated with tumor volume. Table III presents the results of correlations between tumor volumes and texture features in detail.

Discussion

In this study, we demonstrated that different texture features were correlated to certain histological vascular parameters, and that they may reflect change in histological vascular parameters after antiangiogenic therapy.

An *in vivo* metric for the evaluation of antiangiogenic treatment is necessary, because tumor size does not necessarily decrease following antiangiogenic treatment. In this study, tumor volume was not significantly different between the treatment and control groups, although there was a tendency for the treatment group to show delayed tumor growth. No texture features showed significant differences between the two groups, and therefore no specific texture features were considered suitable for differentiating the treated group from the control group.

The texture features showed correlations with histological vascular parameters only in the treated group. MVD was marginally correlated with entropy, VEGF was significantly correlated with homogeneity, and HIF-1α showed the strongest correlation with the 5th percentile value of the ADC values (r=0.844). These differences between the treated and control groups suggest that ADC map texture features may reflect the treatment effect of antiangiogenic therapy, and that they have the potential to allow monitoring of tumor response after antiangiogenic therapy. In particular, as MVD is considered the reference standard for measuring tumor angiogenesis, our findings support the potential use of entropy for response monitoring. However, tumor volume showed marginal association with MVD only and it did not reflect the comprehensive histological vascular changes occurring after antiangiogenic therapy.

Table II. *Correlations between histological vascular parameters and texture features in the treated group.*

Parameters	CD34		HIF-1α		VEGF	
		p-Value		*p*-Value		*p*-Value
Tumor volume	0.461	0.084	–0.406	0.133	–0.041	0.883
Mean value	0.114	0.685	0.644	0.010	0.229	0.412
Skewness	0.050	0.856	–0.580	0.023	–0.471	0.077
Kurtosis	0.100	0.723	–0.531	0.042	–0.399	0.141
Entropy	0.493	0.062	–0.022	0.934	0.004	0.883
Homogeneity	0.224	0.421	0.009	0.974	–0.521	0.046
5th percentile	–0.198	0.478	0.844	<0.001	0.366	0.179
10th percentile	–0.116	0.680	0.728	0.002	0.295	0.286
25th percentile	–0.139	0.620	0.687	0.005	0.294	0.288
50th percentile	–0.057	0.840	0.729	0.002	0.285	0.303
75th percentile	0.132	0.639	0.615	0.015	0.157	0.577
90th percentile	0.111	0.694	0.580	0.023	0.231	0.408
95th percentile	0.125	0.657	0.555	0.032	0.254	0.360

Data are Spearman's correlation coefficients between tumor volumes and texture parameters.

However, as our results were obtained at static time points, there is a need to evaluate serial changes in histological vascular parameters using repeated biopsies after antiangiogenic therapy, and to thereby verify the correlations between histological changes and texture features.

Interestingly, VEGF was significantly higher in the treated group than in the control group. Furthermore, the changes in VEGF resembled the changes in HIF-1α, but with a slight time gap, while there was no such tendency in the control group. This observation corresponds well with previous

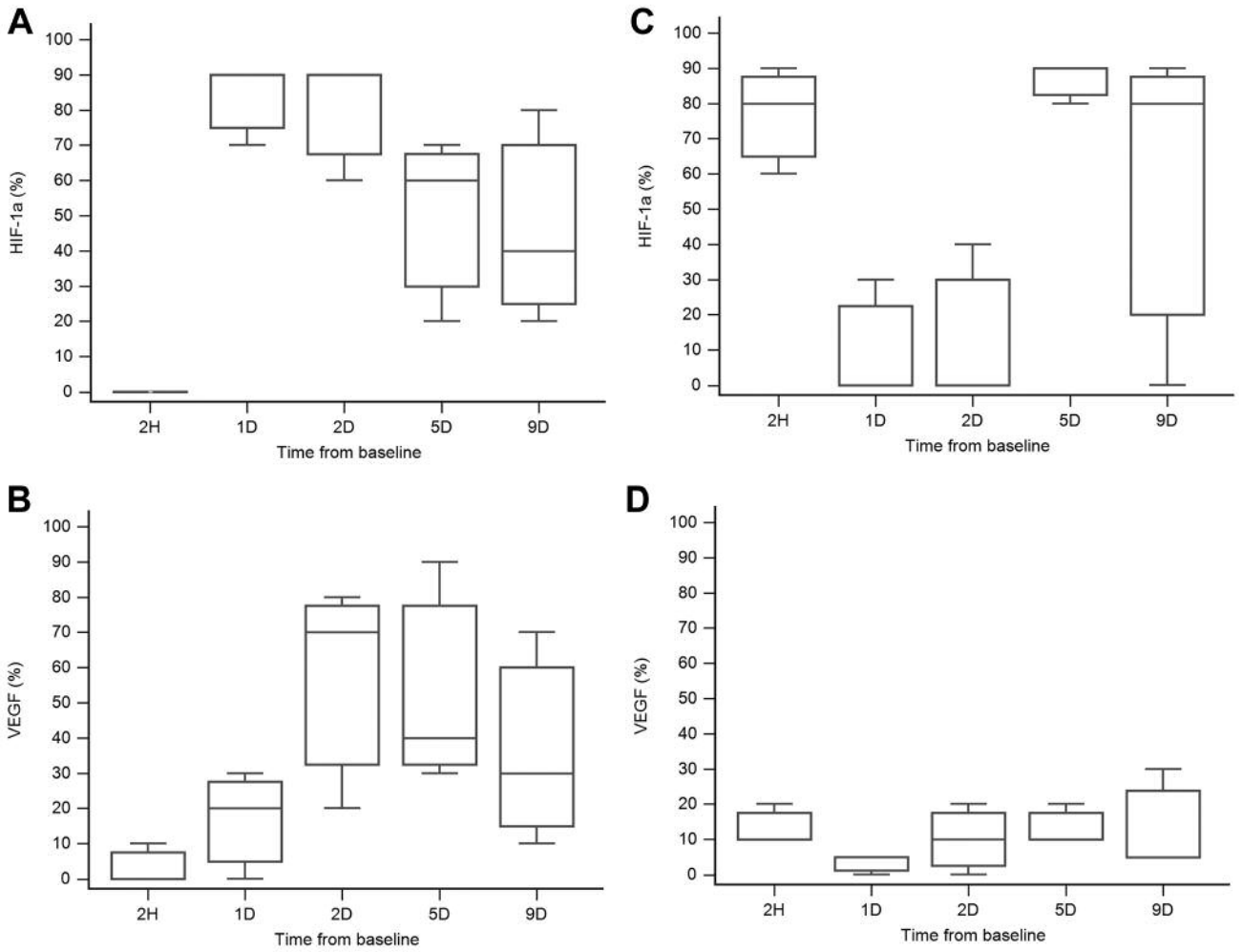

Figure 3. *Serial changes in hypoxia inducible factor-1 alpha (HIF-1α) and vascular endothelial growth factor (VEGF) in the treated and control groups. In the treated group, HIF-1α showed strong activity from follow-up on day 1 (A), and VEGF showed similar changes, but with a slight time difference (B). By contrast, there was no significant association between HIF-1α (C) and VEGF (D) in the control group.*

studies (24-26), which suggested that bevacizumab provokes a more hypoxic environment, which then activates the HIF-1α pathway, leading to the increased expression of VEGF. This finding implies that bevacizumab was effective in the present study.

When the correlations between tumor volume and texture features were assessed, entropy showed a significant correlation with tumor volume in both the treated and control groups, irrespective of whether the original values or the change in ratio between two consecutive time points were used, with correlation coefficients ranging from 0.814 to 0.978. These strong correlations between entropy and tumor volume suggest that entropy can be used as an alternative to tumor volume after antiangiogenic therapy. As this study was not designed to investigate the texture features predictive of an early response to antiangiogenic therapy, we could not evaluate the usefulness of entropy in this regard. Further study is warranted to confirm whether ADC map texture features can predict an early response to antiangiogenic therapy.

The mean ADC value of the tumor was not significantly correlated with tumor volume when changes in ratio between two consecutive time points were used. Although changes in ADC reflect changes in tumor cellularity, cystic change or necrosis occurred frequently during tumor growth in our animal model, and this may have caused the gap between changes in ADC and tumor volume. Previous studies using ADC values have focused on response prediction rather than quantitative correlations (6, 10, 11). Moreover, the present study used MR acquisitions at five time points, and it was therefore more difficult to meet conditions demonstrating a significant correlation. Therefore, for the monitoring of treatment response after antiangiogenic therapy, we believe that entropy is a more stable ADC map-derived texture feature than the mean tumor value.

Table III. *Correlations between tumor volumes and texture features.*

Parameters	Treated group				Control group			
	All values	*p*-Value	Change (ratio)	*p*-Value	All values	*p*-Value	Change (ratio)	*p*-Value
Mean value	–0.626	<0.001	–0.018	0.905	–0.342	0.007	0.072	0.638
Skewness	0.674	<0.001	0.291	0.050	0.562	<0.001	–0.021	0.891
Kurtosis	0.507	<0.001	0.092	0.550	0.497	<0.001	–0.035	0.820
Entropy	0.925	<0.001	0.814	<0.001	0.978	<0.001	0.885	<0.001
Homogeneity	0.087	0.510	0.033	0.831	–0.233	0.07	0.379	0.010
5th percentile	–0.757	<0.001	–0.051	0.738	–0.598	<0.001	–0.155	0.310
10th percentile	–0.743	<0.001	–0.039	0.799	–0.586	<0.001	–0.144	0.344
25th percentile	–0.739	<0.001	–0.162	0.288	–0.525	<0.001	–0.077	0.616
50th percentile	–0.686	<0.001	–0.097	0.527	–0.483	<0.001	0.057	0.711
75th percentile	–0.539	<0.001	–0.025	0.868	–0.240	0.060	0.111	0.467
90th percentile	–0.373	0.003	0.024	0.877	–0.002	0.855	0.182	0.231
95th percentile	–0.223	0.09	0.098	0.520	–0.286	0.441	0.225	0.138

Data are Spearman's correlation coefficients between tumor volumes and texture parameters.

This study has several limitations. First, the study included only a small number of tumors at each time point, and thus features predictive of antiangiogenic treatment were not investigated. However, this work was a feasibility study, and we believe that our results successfully demonstrated correlations between texture features and histological vascular parameters, and the usefulness of ADC map texture analysis. Second, the tumor locations may not have accurately simulated tumor biology in patients in a clinical setting. We decided to perform intramuscular tumor inoculation because of artifacts on ADC maps when tumors are located in the subcutaneous layer. Third, the utility of ADC map texture features was not compared with other imaging modalities such as dynamic contrast-enhanced MR imaging or perfusion CT. Fourth, this study evaluated a single antiangiogenic therapy that was not performed in combination with any other anticancer therapy. However, single antiangiogenic therapy is a more ideal condition for exploring the feasibility of texture analysis on ADC maps.

In conclusion, ADC map texture features may reflect histological vascular changes after antiangiogenic therapy.

Conflicts of Interest

All Authors have no conflicts of interest to disclose.

Authors' Contributions

Study concepts: CMP. Study design: CMP. Data acquisition: SML. Data analysis and interpretation: CMP, SML, MAK, KWL. Statistical analysis: CMP, SML. Manuscript preparation: CMP, SML. Manuscript editing: CMP, SML, KWL. Manuscript review: CMP, SML, KWL, MAK, YSS, JMG. All Authors read and approved the final manuscript.

Acknowledgements

Financial/non-financial disclosures: This research was supported by the Basic Science Research Program through the National Research Foundation of Korea (NRF) funded by the Ministry of Education, Science and Technology (grant number: 2011-0022379).

References

1 Jayson GC, Kerbel R, Ellis LM and Harris AL: Antiangiogenic therapy in oncology: Current status and future directions. Lancet *388(10043)*: 518-529, 2016. PMID: 26853587. DOI: 10.1016/S0140-6736(15)01088-0

2 Burger RA, Brady MF, Bookman MA, Fleming GF, Monk BJ, Huang H, Mannel RS, Homesley HD, Fowler J, Greer BE, Boente M, Birrer MJ, Liang SX and Gynecologic Oncology Group: Incorporation of bevacizumab in the primary treatment of ovarian cancer. N Engl J Med *365(26)*: 2473-2483, 2011. PMID: 22204724. DOI: 10.1056/NEJMoa1104390

3 Sandler A, Gray R, Perry MC, Brahmer J, Schiller JH, Dowlati A, Lilenbaum R and Johnson DH: Paclitaxel-carboplatin alone or with bevacizumab for non-small-cell lung cancer. N Engl J Med *355(24)*: 2542-2550, 2006. PMID: 17167137. DOI: 10.1056/NEJMoa061884

4 Hurwitz H, Fehrenbacher L, Novotny W, Cartwright T, Hainsworth J, Heim W, Berlin J, Baron A, Griffing S, Holmgren E, Ferrara N, Fyfe G, Rogers B, Ross R and Kabbinavar F: Bevacizumab plus irinotecan, fluorouracil, and leucovorin for metastatic colorectal cancer. N Engl J Med *350(23)*: 2335-2342, 2004. PMID: 15175435. DOI: 10.1056/NEJMoa032691

5 Eisenhauer EA, Therasse P, Bogaerts J, Schwartz LH, Sargent D, Ford R, Dancey J, Arbuck S, Gwyther S, Mooney M, Rubinstein L, Shankar L, Dodd L, Kaplan R, Lacombe D and Verweij J: New response evaluation criteria in solid tumours: Revised recist guideline (version 1.1). Eur J Cancer *45(2)*: 228-247, 2009. PMID: 19097774. DOI: 10.1016/j.ejca.2008.10.026

6 Pope WB, Kim HJ, Huo J, Alger J, Brown MS, Gjertson D, Sai V, Young JR, Tekchandani L, Cloughesy T, Mischel PS, Lai A,

Nghiemphu P, Rahmanuddin S and Goldin J: Recurrent glioblastoma multiforme: Adc histogram analysis predicts response to bevacizumab treatment. Radiology *252(1)*: 182-189, 2009. PMID: 19561256. DOI: 10.1148/radiol.2521081534

7 Kim YN, Lee HY, Lee KS, Seo JB, Chung MJ, Ahn MJ, Park K, Kim TS and Yi CA: Dual-energy ct in patients treated with anti-angiogenic agents for non-small cell lung cancer: New method of monitoring tumor response? Korean J Radiol *13(6)*: 702-710, 2012. PMID: 23118568. DOI: 10.3348/ kjr.2012.13.6.702

8 Thoeny HC, De Keyzer F, Vandecaveye V, Chen F, Sun X, Bosmans H, Hermans R, Verbeken EK, Boesch C, Marchal G, Landuyt W and Ni Y: Effect of vascular targeting agent in rat tumor model: Dynamic contrast-enhanced *versus* diffusion-weighted mr imaging. Radiology *237(2)*: 492-499, 2005. PMID: 16192323. DOI: 10.1148/radiol.2372041638

9 Juge L, Doan BT, Seguin J, Albuquerque M, Larrat B, Mignet N, Chabot GG, Scherman D, Paradis V, Vilgrain V, Van Beers BE and Sinkus R: Colon tumor growth and antivascular treatment in mice: Complementary assessment with mr elastography and diffusion-weighted mr imaging. Radiology *264(2)*: 436-444, 2012. PMID: 22692038. DOI: 10.1148/ radiol.12111548

10 Yabuuchi H, Hatakenaka M, Takayama K, Matsuo Y, Sunami S, Kamitani T, Jinnouchi M, Sakai S, Nakanishi Y and Honda H: Non-small cell lung cancer: Detection of early response to chemotherapy by using contrast-enhanced dynamic and diffusion-weighted mr imaging. Radiology *261(2)*: 598-604, 2011. PMID: 21852569. DOI: 10.1148/radiol.11101503

11 Santamaria G, Bargallo X, Fernandez PL, Farrus B, Caparros X and Velasco M: Neoadjuvant systemic therapy in breast cancer: Association of contrast-enhanced mr imaging findings, diffusion-weighted imaging findings, and tumor subtype with tumor response. Radiology *283(3)*: 663-672, 2017. PMID: 27875106. DOI: 10.1148/radiol.2016160176

12 Blazic IM, Lilic GB and Gajic MM: Quantitative assessment of rectal cancer response to neoadjuvant combined chemotherapy and radiation therapy: Comparison of three methods of positioning region of interest for adc measurements at diffusion-weighted mr imaging. Radiology *282(2)*: 418-428, 2017. PMID: 27253423. DOI: 10.1148/radiol.2016151908

13 Baek HJ, Kim HS, Kim N, Choi YJ and Kim YJ: Percent change of perfusion skewness and kurtosis: A potential imaging biomarker for early treatment response in patients with newly diagnosed glioblastomas. Radiology *264(3)*: 834-843, 2012. PMID: 22771885. DOI: 10.1148/radiol.12112120

14 Ueno Y, Forghani B, Forghani R, Dohan A, Zeng XZ, Chamming's F, Arseneau J, Fu L, Gilbert L, Gallix B and Reinhold C: Endometrial carcinoma: MR imaging-based texture model for preoperative risk stratification-a preliminary analysis. Radiology *284(3)*: 748-757, 2017. PMID: 28493790. DOI: 10.1148/radiol.2017161950

15 Vermeulen PB, Gasparini G, Fox SB, Colpaert C, Marson LP, Gion M, Belien JA, de Waal RM, Van Marck E, Magnani E, Weidner N, Harris AL and Dirix LY: Second international consensus on the methodology and criteria of evaluation of angiogenesis quantification in solid human tumours. Eur J Cancer *38(12)*: 1564-1579, 2002. PMID: 12142044.

16 Wang GL, Jiang BH, Rue EA and Semenza GL: Hypoxia-inducible factor 1 is a basic-helix-loop-helix-pas heterodimer regulated by cellular o2 tension. Proc Natl Acad Sci USA *92(12)*: 5510-5514, 1995. PMID: 7539918.

17 Zhong H, De Marzo AM, Laughner E, Lim M, Hilton DA, Zagzag D, Buechler P, Isaacs WB, Semenza GL and Simons JW: Overexpression of hypoxia-inducible factor 1alpha in common human cancers and their metastases. Cancer Res *59(22)*: 5830-5835, 1999. PMID: 10582706.

18 Fondevila C, Metges JP, Fuster J, Grau JJ, Palacin A, Castells A, Volant A and Pera M: P53 and vegf expression are independent predictors of tumour recurrence and survival following curative resection of gastric cancer. Br J Cancer *90(1)*: 206-215, 2004. PMID: 14710231. DOI: 10.1038/sj.bjc.6601455

19 Alvarez E, Westmore M, Galvin RJ, Clapp CL, Considine EL, Smith SJ, Keyes K, Iversen PW, Delafuente DM, Sulaimon S, Zambrano C, Ma L, Sato M, Martin TJ, Teicher BA and Galbreath EJ: Properties of bisphosphonates in the 13762 rat mammary carcinoma model of tumor-induced bone resorption. Clin Cancer Res *9(15)*: 5705-5713, 2003. PMID: 14654555.

20 Song YS, Park CM, Lee SM, Park SJ, Cho HR, Choi SH, Lee JM, Kiefer B and Goo JM: Reproducibility of histogram and texture parameters derived from intravoxel incoherent motion diffusion-weighted mri of fn13762 rat breast carcinomas. Anticancer Res *34(5)*: 2135-2144, 2014. PMID: 24778015.

21 Kim YH, Kim MA, Park IA, Park WY, Kim JW, Kim SC, Park NH, Song YS and Kang SB: Vegf polymorphisms in early cervical cancer susceptibility, angiogenesis, and survival. Gynecol Oncol *119(2)*: 232-236, 2010. PMID: 20797778. DOI: 10.1016/j.ygyno.2010.07.035

22 Kim JI, Lee HJ, Goo JM, Kim MA and Chung DH: Correlation of volumetric perfusion ct parameters with hypoxia inducible factor-1 alpha expression in a rabbit vx2 tumor model. Acta Radiol *57(6)*: 708-715, 2016. PMID: 26339038. DOI: 10.1177/0284185115603243

23 Mattern J, Koomagi R and Volm M: Vascular endothelial growth-factor expression and angiogenesis in nonsmall cell lung carcinomas. Int J Oncol *6(5)*: 1059-1062, 1995. PMID: 21556640.

24 Keunen O, Johansson M, Oudin A, Sanzey M, Rahim SA, Fack F, Thorsen F, Taxt T, Bartos M, Jirik R, Miletic H, Wang J, Stieber D, Stuhr L, Moen I, Rygh CB, Bjerkvig R and Niclou SP: Anti-vegf treatment reduces blood supply and increases tumor cell invasion in glioblastoma. Proc Natl Acad Sci USA *108(9)*: 3749-3754, 2011. PMID: 21321221. DOI: 10.1073/pnas.1014480108

25 Miyazaki S, Kikuchi H, Iino I, Uehara T, Setoguchi T, Fujita T, Hiramatsu Y, Ohta M, Kamiya K, Kitagawa K, Kitagawa M, Baba S and Konno H: Anti-vegf antibody therapy induces tumor hypoxia and stanniocalcin 2 expression and potentiates growth of human colon cancer xenografts. Int J Cancer *135(2)*: 295-307, 2014. PMID: 24375080. DOI: 10.1002/ijc.28686

26 Xu H, Rahimpour S, Nesvick CL, Zhang X, Ma J, Zhang M, Zhang G, Wang L, Yang C, Hong CS, Germanwala AV, Elder JB, Ray-Chaudhury A, Yao Y, Gilbert MR, Lonser RR, Heiss JD, Brady RO, Mao Y, Qin J and Zhuang Z: Activation of hypoxia signaling induces phenotypic transformation of glioma cells: Implications for bevacizumab antiangiogenic therapy. Oncotarget *6(14)*: 11882-11893, 2015. PMID: 25957416. DOI: 10.18632/oncotarget.3592

Received February 2, 2019
Revised March 15, 2019
Accepted March 20, 2019